Eur. Phys. J. C (2017) 77:640
DOI 10.1140/epjc/s10052-017-5203-0

THE EUROPEAN PHYSICAL JOURNAL C

Regular Article - Theoretical Physics

Helicity-dependent generalized parton distributions for nonzero skewness

Chandan Mondal[a]

Institute of Modern Physics, Chinese Academy of Sciences, Lanzhou 730000, China

Received: 14 July 2017 / Accepted: 4 September 2017 / Published online: 22 September 2017

Abstract We investigate the helicity-dependent generalized parton distributions (GPDs) in momentum as well as transverse position (impact) spaces for the u and d quarks in a proton when the momentum transfer in both the transverse and the longitudinal directions are nonzero. The GPDs are evaluated using the light-front wave functions of a quark–diquark model for nucleon where the wave functions are constructed by the soft-wall AdS/QCD correspondence. We also express the GPDs in the boost-invariant longitudinal position space.

1 Introduction

Generalized parton distributions (GPDs) play a crucial role in our understanding of the structure of the hadron in terms of the fundamental building blocks of QCD, the quarks and gluons. The GPDs (see [1–3] for reviews on GPDs) encode a wealth of information about the three dimensional spatial structure of the hadron as well as the spin and orbital angular momentum of the constituents. The GPDs are experimentally accessible in the exclusive processes like deeply virtual Compton scattering (DVCS) or vector meson productions. At the parton level one can distinguish three kinds of parton distributions functions (PFDs): the unpolarized, the helicity distribution, and the transversity which are the functions of longitudinal momentum faction carried by the parton (x) only. The GPDs being functions of three variables x, square of the total momentum transferred t, and the longitudinal momentum transferred ζ so-called skewness in the process contain more information than the ordinary PDFs. In the forward limit, GPDs reduce to PDFs whereas the first moments of GPDs give the form factors which are accessible in exclusive processes. In parallel to three PDFs, one can define three generalized distributions namely, the unpolarized, helicity, and transversity distributions. The unpolarized and helicity GPDs are chiral-even and the transversity GPDs are chiral-odd. At leading twist, four chiral-even GPDs occur. Two of them are usually called unpolarized GPDs (H and E). The other two are usually called helicity-dependent or polarized GPDs which are labeled $\widetilde{H}$ and $\widetilde{E}$. The first of them gives in forward linit the polarized quark density, the second is a spin-flip distribution which implies a change of the spin of the target. At zero skewness ($\zeta = 0$), via Fourier transform with respect to the momentum transfer in the transverse direction $\mathbf{\Delta}_\perp$, GPDs transform to the impact parameter-dependent parton distributions. Unlike the GPDs themselves, impact parameter-dependent parton distributions have the interpretation of a density of partons with longitudinal momentum fraction x and transverse distance $b = |\mathbf{b}_\perp|$ from the protons center, where $\mathbf{b}_\perp$ is the conjugate variable to $\mathbf{\Delta}_\perp$ and satisfy the positivity condition [4–7]. The second moment of the GPDs corresponds to the gravitational form factors which are again related to the partonic contribution to the angular momentum of nucleon at the $t \to 0$ limit [8]. When one considers transversely polarized nucleons, the impact parameter-dependent PDFs get distorted and the transverse distortion can also be connected with Ji's angular momentum relation. For transversely polarized state, an interesting interpretation of Ji's angular momentum sum rule [8] was obtained in terms of the impact parameter-dependent PDFs in [4]. Transverse distortion arises due to the GPD E for the unpolarized quark, which is related to the anomalous magnetic moment of the quarks. But in the case of transversely polarized quark, the linear combination of chiral-odd GPDs $(2\widetilde{H}_T + E_T)$ plays a role similar to the GPD E as for the unpolarized quark distributions. The helicity-dependent GPDs $\widetilde{H}$ in impact parameter space reflects the difference in the density of quarks with helicity equal or opposite to the proton helicity [9–11]. For nonzero skewness, the GPDs can also be represented in the longitudinal position space by taking Fourier transform of the GPDs with respect to ζ [12–19].

[a] e-mail: mondal@impcas.ac.cn

Unlike the PFDs and form factors, it is always very difficult to measure the GPDs which can be accessed in DVCS scattering [20,21]. First experimental DVCS results in terms of the beam spin asymmetry have been presented by HERMES at DESY [22] and CLAS at JLab [23]. Since then, many more results have become available from the measurements performed by the Hall A and Hall B/CLAS collaborations at JLab [24–27] and the H1, ZEUS and HERMES collaborations at DESY [28–34]. Exclusive production of ω meson [35], and ρ^0 mesons [36] by scattering muons off transversely polarized proton has been measured in a very recent COMPASS experiments. The target spin asymmetries measured in these experiments agree well with GPD-based model calculations. There has been proposals to get access to the GPDs through diffractive double meson production [37–39]. The role of the GPDs in hard exclusive electroproduction of pseudo-scalar mesons [40] as well as in leptoproduction of vector mesons [41] have been investigated within the framework of the handbag approach.

Since the nonperturbative properties of hadrons are always very difficult to evaluate from QCD first principles, there have been numerous attempts to gain insight into the hadron structure by studying QCD inspired models. Several theoretical predictions for the GPDs have been produced by using different descriptions of hadron structure, such as bag models [42,43], soliton models [3,44,45], light-front models [46–48], constituent quark models (CQM) [49–52], and AdS/QCD models [53–55]. Recently, the GPDs for nonzero skewness in AdS/QCD framework has been investigated in [56,57]. In [58], the helicity-dependent GPDs for nonzero skewness in a CQM have been studied considering the Dokshitzer Gribov Lipatov Altarelli Parisi (DGLAP) region whereas these GPDs in CQM with a kinematical range corresponding to both the DGLAP and the Efremov–Radyushkin–Brodsky–Lepage (ERBL) regions have been investigated in [59]. The helicity-dependent twist-two and twist-three GPDs in light-front Hamiltonian QCD for a massive dressed quark target has been presented in [48]. The general properties of GPDs in QED models have been studied in both momentum and transverse position as well as longitudinal position spaces [12,60]; the impact parameter representation of the GPDs have been investigated in a QED model of a dressed electron [13]. The moments of the GPDs have been calculated on lattice [61–65]. In this work, we consider a light-front quark–diquark model recently proposed by Gutsche et al. [66] where the light-front wave functions are modeled from the two particle wave functions obtained in a soft-wall model of AdS/QCD correspondence [67,68]. This model is consistent with Drell–Yan–West relation and has been shown to reproduce many interesting nucleon properties. So far the quark–diquark model has been successfully applied to describe various aspect of nucleon properties e.g., electromagnetic and gravitational form factor, GPDs, TMDs, charge densities, longitudinal momentum densities etc. [18,19,69–74]. More importantly, since the AdS/QCD formalism is a semiclassical approach to solving nonperturbative QCD, one can expect that the wave functions modeled by AdS/QCD correspondence encode the nonperturbative information of the nucleon and thus the wave functions are suitable to study the nonperturbative properties like GPDs, TMDs. It should be mentioned here that recently TMDs of pion have been evaluated using a model inspired by AdS/QCD correspondence [75]. Here, we investigate the skewed helicity-dependent GPDs in both momentum and transverse and longitudinal position space in this light-front quark–diquark model inspired by AdS/QCD. We also present the quark transverse distributions for the u and d quarks in a longitudinally polarized nucleon.

The paper is organized as follows. A brief introduction of the nucleon light-front wave functions of the quark–diquark model has been given in Sect. 2. In Sect. 3, we present the overlap formalism of the helicity-dependent GPDs and show the results for proton GPDs of u and d quarks in momentum space. The GPDs in the transverse as well as the longitudinal impact parameter space are shown in Sects. 4.1 and 4.2. The quark transverse distributions in the nucleon with longitudinal polarization $\Lambda(=+1)$ are presented in Sect. 4.3. Finally we provide a summary all the results in Sect. 5.

2 Light-front quark–diquark model constructed by AdS/QCD

Here we adopt the generic ansatz for the light-front quark–diquark model for the nucleons [66] where the light-front wave functions are modeled from the solution of soft-wall AdS/QCD. In this model, one contemplates the three valence quarks of the nucleons as an effective system composed of a fermion (quark) and a composite state of diquark (boson) based on one loop quantum fluctuations. Then the 2-particle Fock-state expansion for proton spin components, $J^z=+\frac{1}{2}$ and $J^z=-\frac{1}{2}$ in a frame where the transverse momentum of proton vanishes i.e. $P\equiv\left(P^+,\frac{M_n^2}{P^+},\mathbf{0}_\perp\right)$, are written as

$$
\begin{aligned}
|P;+\rangle &= \sum_q \int \frac{\mathrm{d}x\ \mathrm{d}^2\mathbf{k}_\perp}{2(2\pi)^3\sqrt{x(1-x)}} \\
&\quad\times\Bigg[\psi^+_{+q}(x,\mathbf{k}_\perp)|+\frac{1}{2},0;xP^+,\mathbf{k}_\perp\rangle \\
&\quad+\psi^+_{-q}(x,\mathbf{k}_\perp)|-\frac{1}{2},0;xP^+,\mathbf{k}_\perp\rangle\Bigg], \qquad (1)\\
|P;-\rangle &= \sum_q \int \frac{\mathrm{d}x\ \mathrm{d}^2\mathbf{k}_\perp}{2(2\pi)^3\sqrt{x(1-x)}}
\end{aligned}
$$

$$\times\Big[\psi^{-}_{+q}(x,\mathbf{k}_\perp)|+\frac{1}{2},0;xP^+,\mathbf{k}_\perp\rangle$$
$$+\psi^{-}_{-q}(x,\mathbf{k}_\perp)|-\frac{1}{2},0;xP^+,\mathbf{k}_\perp\rangle\Big]. \quad (2)$$

However, for nonzero transverse momentum of proton, i.e. $\mathbf{P}_\perp \neq 0$, the physical transverse momenta of quark and diquark are $\mathbf{p}^q_\perp = x\mathbf{P}_\perp + \mathbf{k}_\perp$ and $\mathbf{p}^D_\perp = (1-x)\mathbf{P}_\perp - \mathbf{k}_\perp$, respectively, where $\mathbf{k}_\perp$ represents the relative transverse momentum of the constituents. $\psi^{\lambda_N}_{\lambda_q q}(x,\mathbf{k}_\perp)$ are the light-front wave functions with nucleon helicities $\lambda_N = \pm$ and for the struck quark $\lambda_q = \pm$; plus and minus correspond to $+\frac{1}{2}$ and $-\frac{1}{2}$, respectively. The light-front wave functions are given by [66]

$$\begin{aligned}
\psi^{+}_{+q}(x,\mathbf{k}_\perp) &= \varphi^{(1)}_q(x,\mathbf{k}_\perp),\\
\psi^{+}_{-q}(x,\mathbf{k}_\perp) &= -\frac{k^1+ik^2}{xM_n}\varphi^{(2)}_q(x,\mathbf{k}_\perp),\\
\psi^{-}_{+q}(x,\mathbf{k}_\perp) &= \frac{k^1-ik^2}{xM_n}\varphi^{(2)}_q(x,\mathbf{k}_\perp),\\
\psi^{-}_{-q}(x,\mathbf{k}_\perp) &= \varphi^{(1)}_q(x,\mathbf{k}_\perp).
\end{aligned} \quad (3)$$

Here, $\varphi^{(i=1,2)}_q(x,\mathbf{k}_\perp)$ are the modified wave functions which are constructed by soft-wall AdS/QCD, after introducing the parameters $a^{(i)}_q$ and $b^{(i)}_q$ for quark q,

$$\varphi^{(i)}_q(x,\mathbf{k}_\perp) = N^{(i)}_q\frac{4\pi}{\kappa}\sqrt{\frac{\log(1/x)}{1-x}}x^{a^{(i)}_q}(1-x)^{b^{(i)}_q} \times\exp\Big[-\frac{\mathbf{k}^2_\perp}{2\kappa^2}\frac{\log(1/x)}{(1-x)^2}\Big]. \quad (4)$$

$\varphi^{(i)}_q(x,\mathbf{k}_\perp)$ reduces to the AdS/QCD solution when $a^{(i)}_q = b^{(i)}_q = 0$ [68]. In this work, we take the AdS/QCD scale parameter $\kappa = 0.4$ GeV, obtained by fitting the nucleon form factors in the soft-wall model of AdS/QCD [55,76]. The parameters $a^{(i)}_q$ and $b^{(i)}_q$ with the constants $N^{(i)}_q$ are obtained by fitting the electromagnetic properties of the nucleons: $F^q_1(0) = n_q$ and $F^q_2(0) = \kappa_q$ where $n_u = 2$ and $n_d = 1$, the number of valence u and d quarks in proton and the anomalous magnetic moments for the u and d quarks are $\kappa_u = 1.673$ and $\kappa_d = -2.033$ [19]. The parameters are given by $a^{(1)}_u = 0.020$, $a^{(1)}_d = 0.10$, $b^{(1)}_u = 0.022$, $b^{(1)}_d = 0.38$, $a^{(2)}_u = 1.05$, $a^{(2)}_d = 1.07$, $b^{(2)}_u = -0.15$, $b^{(2)}_d = -0.20$, $N^{(1)}_u = 2.055$, $N^{(1)}_d = 1.7618$, $N^{(2)}_u = 1.322$, $N^{(2)}_d = -2.4827$.

3 Helicity-dependent generalized parton distributions

The helicity-dependent GPDs are defined as off-forward matrix elements of the bilocal operator of light-front correlation functions of the axial-vector current [1,2,8,77]

$$\frac{1}{2}\int\frac{dz^-}{2\pi}e^{ixP^+z^-} \times\langle p',\lambda'|\,\bar\psi(-\tfrac{1}{2}z)\,\gamma^+\gamma_5\,\psi(\tfrac{1}{2}z)\,|p,\lambda\rangle\Big|_{z^+=0,\,\mathbf{z}_T=0}$$
$$=\frac{1}{2P^+}\bar u(p',\lambda')\Big[\widetilde H^q\,\gamma^+\gamma_5+\widetilde E^q\,\frac{\gamma_5\Delta^+}{2M}\Big]u(p,\lambda), \quad (5)$$

where p (p') and λ (λ') denote the proton momenta and the helicity of the initial (final) state of proton, respectively. The kinematical variables in the symmetric frame are

$$P^\mu = \frac{(p+p')^\mu}{2},\quad \Delta^\mu = p'^\mu - p^\mu,\quad \zeta = -\Delta^+/2P^+, \quad (6)$$

and $t = \Delta^2$. For $\zeta = 0, t = -\mathbf{\Delta}^2_\perp$. We work in the light-front gauge $A^+ = 0$, so that the gauge link appearing in between the quark fields in Eq. (5) is unity. The quark helicity conserving distributions can be related to the following matrix elements [9,77]:

$$\begin{aligned}
A_{\lambda'+,\lambda+} &= \int\frac{dz^-}{2\pi}e^{i\bar xP^+z^-}\langle p',\lambda'|\,\mathcal{O}_{+,+}(z)\,|p,\lambda\rangle\Big|_{z^+=\mathbf{z}_\perp=0},\\
A_{\lambda'-,\lambda-} &= \int\frac{dz^-}{2\pi}e^{i\bar xP^+z^-}\langle p',\lambda'|\,\mathcal{O}_{-,-}(z)\,|p,\lambda\rangle\Big|_{z^+=\mathbf{z}_\perp=0},
\end{aligned} \quad (7)$$

where the operators $O_{+,+}$ and $O_{-,-}$ occurring in the definitions of the quark distributions are

$$\begin{aligned}
\mathcal{O}_{+,+} &= \frac{1}{4}\,\bar\psi\,\gamma^+(1+\gamma_5)\,\psi,\\
\mathcal{O}_{-,-} &= \frac{1}{4}\,\bar\psi\,\gamma^+(1-\gamma_5)\,\psi.
\end{aligned} \quad (8)$$

One can explicitly derive the following relations in the reference frame where the momenta $\mathbf{p}$ and $\mathbf{p}'$ lie in the $x-z$ plane [77]:

$$\begin{aligned}
A_{++,++} &= \sqrt{1-\zeta^2}\left(\frac{H^q+\widetilde H^q}{2}-\frac{\zeta^2}{1-\zeta^2}\,\frac{E^q+\widetilde E^q}{2}\right),\\
A_{-+,-+} &= \sqrt{1-\zeta^2}\left(\frac{H^q-\widetilde H^q}{2}-\frac{\zeta^2}{1-\zeta^2}\,\frac{E^q-\widetilde E^q}{2}\right),\\
A_{++,-+} &= -\epsilon\,\frac{\sqrt{t_0-t}}{2m}\,\frac{E^q-\zeta\widetilde E^q}{2},\\
A_{-+,++} &= \epsilon\,\frac{\sqrt{t_0-t}}{2m}\,\frac{E^q+\zeta\widetilde E^q}{2},
\end{aligned} \quad (9)$$

where $\epsilon = \mathrm{sgn}(D^1)$, and D^1 is the x-component of $D^\alpha = P^+\Delta^\alpha - \Delta^+P^\alpha$ where $D^1 = 0$ corresponds to $t = t_0$. For given ζ, the minimum value of $-t$ is $-t_0 = 4m^2\zeta^2/(1-\zeta^2)$. Due to parity invariance, one has the relations $A_{-\lambda'-\mu',-\lambda-\mu} = (-1)^{\lambda'-\mu'-\lambda+\mu}\,A_{\lambda'\mu',\lambda\mu}$ for definite quark helicities μ and μ'. We can now compute the helicity-dependent GPDs $\widetilde H^q$ and $\widetilde E^q$ using the relations in Eq. (9) as

$$\widetilde{H}^q = \frac{1}{\sqrt{1-\zeta^2}} T_1^q + \frac{2M\zeta}{\sqrt{t_0 - t(1-\zeta^2)}} T_2^q, \tag{10}$$

$$\widetilde{E}^q = \frac{2M}{\epsilon\zeta\sqrt{t_0 - t}} T_2^q, \tag{11}$$

where the matrix elements T_i^q, in terms of the quark helicity basis, are given by

$$\begin{aligned} T_1^q &= A_{++,++} - A_{-+,-+}, \\ T_2^q &= A_{++,-+} + A_{-+,++}. \end{aligned} \tag{12}$$

3.1 Overlap formalism

We evaluate the helicity-dependent GPDs in light-front quark–diquark model using the overlap representation of light-front wave functions. We consider the DGLAP region for our discussion. This kinematical domain, i.e., $\zeta < x < 1$ where x is the light-front longitudinal momentum fraction carried by the struck quark and ζ is the skewness, corresponds to the situation where one removes a quark from the initial proton with light-front longitudinal momentum $(x+\zeta)P^+$ and re-insert it into the final proton with longitudinal momentum $(x-\zeta)P^+$. The particle number remain conserved in this kinematical region which describes the diagonal $n \to n$ overlaps. The matrix elements T_i^q in the diagonal $2 \to 2$ overlap representation, in terms of light-front wave functions in the quark–diquark model, are given by

$$\begin{aligned} T_1^q = \int \frac{\mathrm{d}^2\mathbf{k}_\perp}{16\pi^3} \Big[& \psi_{+q}^{+*}(x', \mathbf{k}'_\perp)\psi_{+q}^{+}(x'', \mathbf{k}''_\perp) \\ & - \psi_{+q}^{-*}(x', \mathbf{k}'_\perp)\psi_{+q}^{-}(x'', \mathbf{k}''_\perp) \Big], \end{aligned} \tag{13}$$

$$\begin{aligned} T_2^q = \int \frac{\mathrm{d}^2\mathbf{k}_\perp}{16\pi^3} \Big[& \psi_{+q}^{+*}(x', \mathbf{k}'_\perp)\psi_{+q}^{-}(x'', \mathbf{k}''_\perp) \\ & + \psi_{+q}^{-*}(x', \mathbf{k}'_\perp)\psi_{+q}^{+}(x'', \mathbf{k}''_\perp) \Big], \end{aligned} \tag{14}$$

where for the final struck quark

$$x' = \frac{x-\zeta}{1-\zeta}, \quad \mathbf{k}'_\perp = \mathbf{k}_\perp + (1-x')\frac{\boldsymbol{\Delta}_\perp}{2}, \tag{15}$$

and for the initial struck quark

$$x'' = \frac{x+\zeta}{1+\zeta}, \quad \mathbf{k}''_\perp = \mathbf{k}_\perp - (1-x'')\frac{\boldsymbol{\Delta}_\perp}{2}. \tag{16}$$

Using the light-front wave functions of the quark–diquark model given in Eq. (3), the explicit calculation of the matrix elements T_i^q gives

$$\begin{aligned} T_1^q(x,\zeta,t) &= \Delta q \frac{\mathcal{T}_1^q(x,\zeta,t)}{\mathcal{I}(0)}, \\ T_2^q(x,\zeta,t) &= \mathcal{T}_2^q(x,\zeta,t), \end{aligned} \tag{17}$$

with $\mathcal{I}(0) = \int_0^1 \mathrm{d}x\ \mathcal{T}_1^q(x,0,0)$, and Δq is the axial charge of quark q. The functions $\mathcal{T}_i^q(x,\zeta,t)$ are given by

$$\begin{aligned} \mathcal{T}_1^q = \frac{1}{\kappa^2}\Big[\frac{\log x' \log x''}{(1-x')(1-x'')}\Big]^{1/2} \Big[& (N_q^{(1)})^2 (x'x'')^{a_q^{(1)}} \\ & \times \{(1-x')(1-x'')\}^{b_q^{(1)}} \frac{1}{A} \\ & - (N_q^{(2)})^2 \frac{1}{M_n^2} (x'x'')^{a_q^{(2)}-1} \\ & \times \{(1-x')(1-x'')\}^{b_q^{(2)}} \\ & \times \Big\{ \frac{1}{A^2} + \Big(\frac{B^2}{4A^2} - \frac{1}{4}(1-x') \times (1-x'') \\ & + \frac{B}{4A}(x''-x') \Big) \frac{Q^2}{A} \Big\} \Big] \\ & \times \exp\Big[Q^2 \Big(C + \frac{B^2}{4A} \Big) \Big], \end{aligned} \tag{18}$$

$$\begin{aligned} \mathcal{T}_2^q = \frac{N_q^{(1)} N_q^{(2)}}{\kappa^2}\Big[\frac{\log x' \log x''}{(1-x')(1-x'')}\Big]^{1/2} & \\ \times \frac{1}{M_n} \Big[& (x')^{a_q^{(1)}} \times (1-x')^{b_q^{(1)}} (x'')^{a_q^{(2)}-1} (1-x'')^{b_q^{(2)}} \\ & \times \Big(\frac{BQ}{2A^2} - \frac{Q}{2A}(1-x'') \Big) \\ & + (x')^{a_q^{(2)}-1} (1-x')^{b_q^{(2)}} (x'')^{a_q^{(1)}} \\ & \times (1-x'')^{b_q^{(1)}} \Big(\frac{BQ}{2A^2} + \frac{Q}{2A}(1-x') \Big) \Big] \\ & \times \exp\Big[Q^2 \Big(C + \frac{B^2}{4A} \Big) \Big], \end{aligned} \tag{19}$$

where $\Delta_\perp^2 = Q^2 = -t(1-\zeta^2) - 4M_n^2\zeta^2$. A, B and C are functions of x' and x'',

$$\begin{aligned} A = A(x,x') &= -\frac{\log x'}{2\kappa^2(1-x)^2} - \frac{\log x''}{2\kappa^2(1-x')^2}, \\ B = B(x,x') &= \frac{\log x'}{2\kappa^2(1-x)} - \frac{\log x''}{2\kappa^2(1-x')}, \\ C = C(x,x') &= \frac{1}{4}\Big[\frac{\log x'}{2\kappa^2} + \frac{\log x''}{2\kappa^2} \Big]. \end{aligned} \tag{20}$$

Using the matrix elements calculated in Eqs. (13) and (14) we compute the helicity-dependent GPDs in Eq. (11). The GPD $\widetilde{H}^q$ are suitably normalize by the axial charge Δq where the experimental values of $\Delta u = 0.82$, and $\Delta d = -0.45$ [78,79].

The helicity-dependent GPDs for nonzero skewness ($\zeta \neq 0$) for u and d quarks are shown in Figs. 1, 2 and 3. In Fig. 1, the GPDs are shown as functions of x and $-t$ and a fixed value of $\zeta = 0.2$ whereas in Fig. 2, we plot the GPDs for a fixed value of $-t = 0.7$ GeV^2 but different values of ζ. One can notice that the height of the peaks of the distributions increase and move to higher x with increasing ζ for fixed $-t$. The GPDs fall to zero at $x = \zeta$ when ζ is very low or the value of $-t$ is high. The reason is that in our approach we

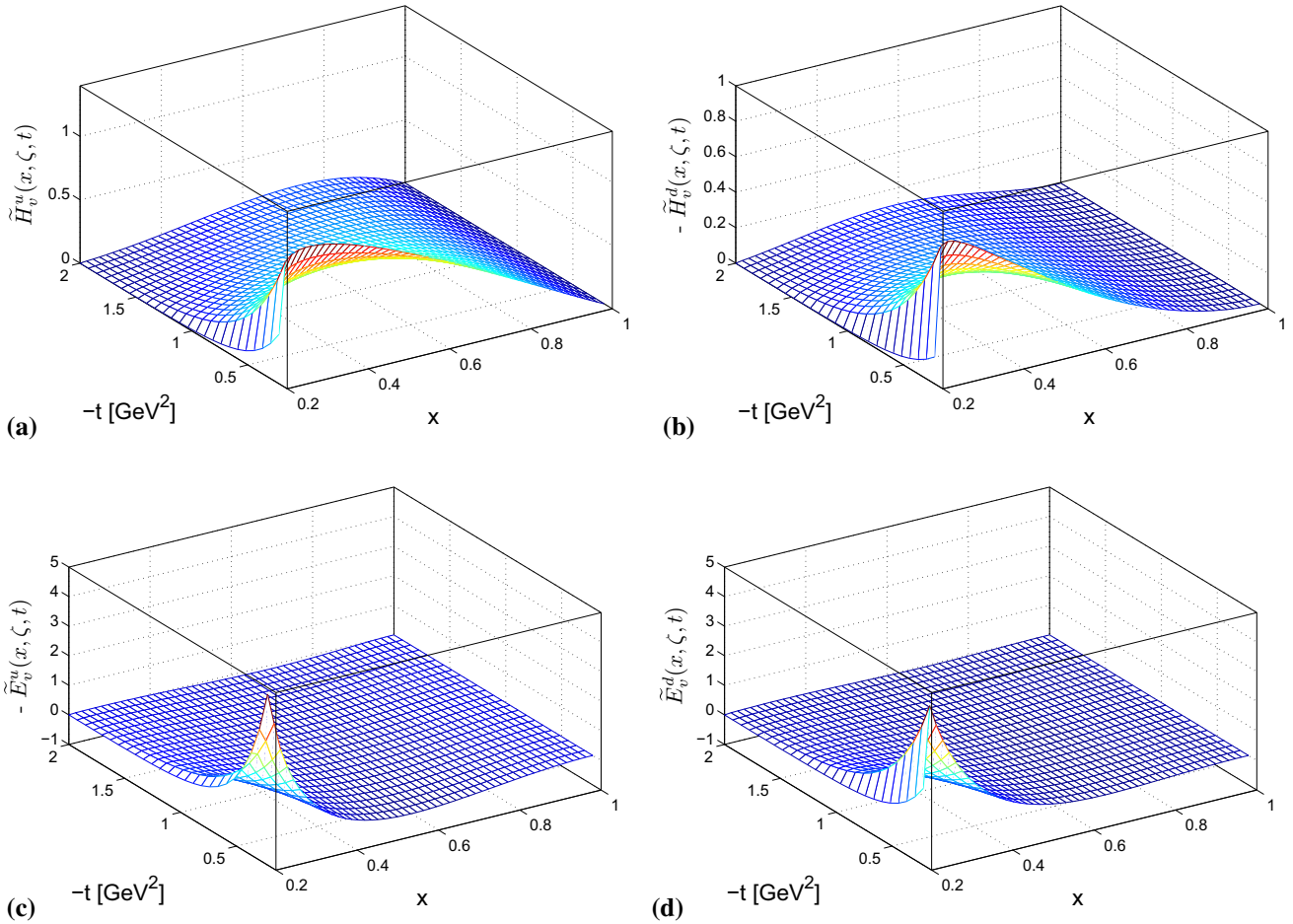

Fig. 1 (Color online) Plots of helicity-dependent GPDs for the nonzero skewness as functions of x and $-t$, and for a fixed value of $\zeta = 0.2$. **a** $\widetilde{H}_v^u$, **b** $\widetilde{H}_v^d$ and **c** $\widetilde{E}_v^u$, **d** $\widetilde{E}_v^d$; for $\zeta = 0.2$ the minimum value of $-t = -t_0 = 0.147$ GeV^2

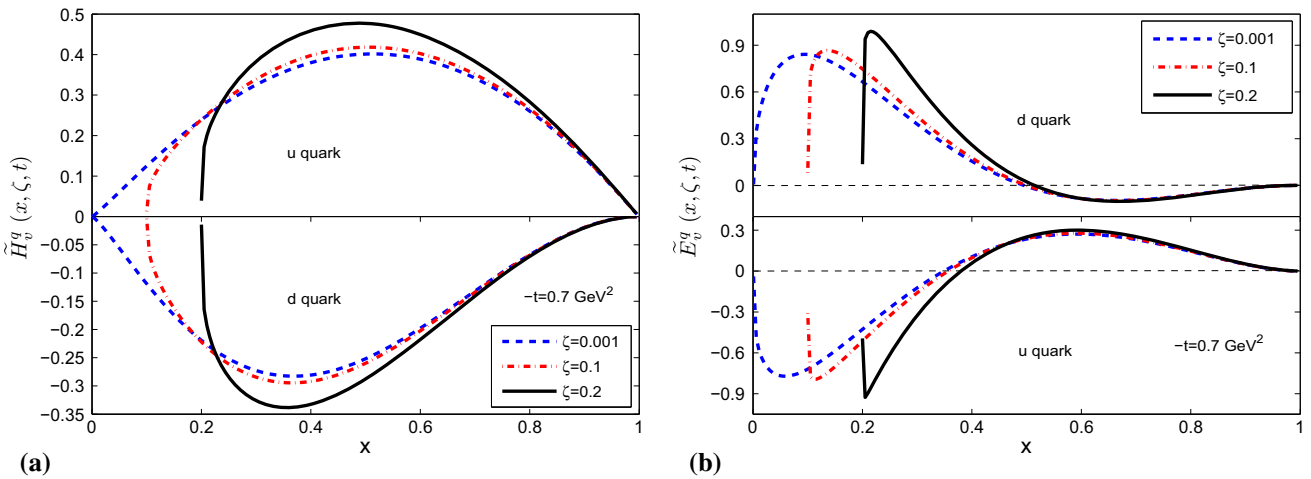

Fig. 2 (Color online) Plots of helicity-dependent GPDs for the nonzero skewness vs. x and different values of ζ, for a fixed value of $t = -0.7$ GeV^2. **a** $\widetilde{H}_v^q$ and **b** $\widetilde{E}_v^q$; q stands for the u and d quark

consider the contribution only from the valence quarks. Since the quark–diquark model itself depends only on the valence quarks; we cannot evaluate the total (sea + valence) GPDs in this model. A similar behavior of the helicity-dependent GPDs has been found in the relativistic constituent quark model calculated in [58]. Also, the ERBL region, i.e. $x < \zeta$

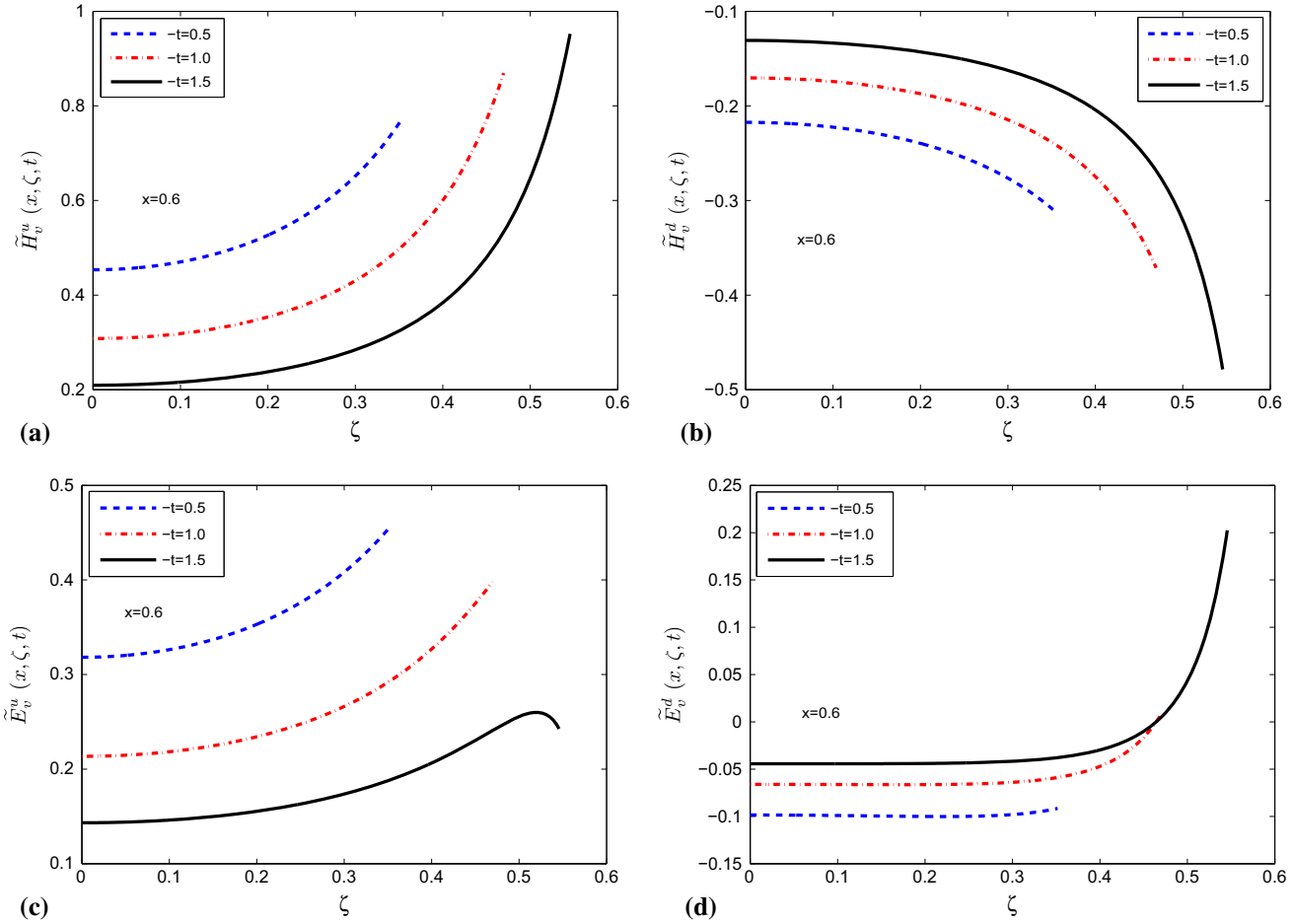

Fig. 3 (Color online) Plots of helicity-dependent GPDs for the nonzero skewness vs. ζ and different values of $-t$ in GeV^2, for a fixed value of $x = 0.6$. The left panel is for the u quark and the right panel is for the d quark

where quark–antiquark pair creation and annihilation are involved is not included in this model. In Fig. 3, we show the GPDs as functions of ζ for fixed x and different values of $-t$. The GPDs rise smoothly as ζ increases for all t values and GPDs have different values at $\zeta = 0$ for different values of $-t$. Similar behaviors have also been observed for the unpolarized and chiral-odd GPDs (except $\widetilde{E}_T$; it is odd in ζ) in the quark–diquark model [18,19], a phenomenological QED model [12]. It can also be noticed that $\widetilde{E}^u(x,\zeta,t)$ shows a markedly different behavior from the other GPDs. $\widetilde{E}^u(x,\zeta,t)$ rises smoothly as ζ increases but the magnitude at $\zeta_{\max} = \sqrt{(-t)/(-t+4M_n^2)}$ decreases with increasing $-t$.

3.2 Mellin moments of helicity-dependent GPDs

The Mellin moments of the valence GPDs are defined as

$$\widetilde{H}^q_{n0}(t) = \int_0^1 \mathrm{d}x x^{n-1} \widetilde{H}^q(x,0,t), \tag{21}$$

where the index $n = 1, 2, 3$ etc., and the second subscript implies that the moments are evaluated at zero skewness.

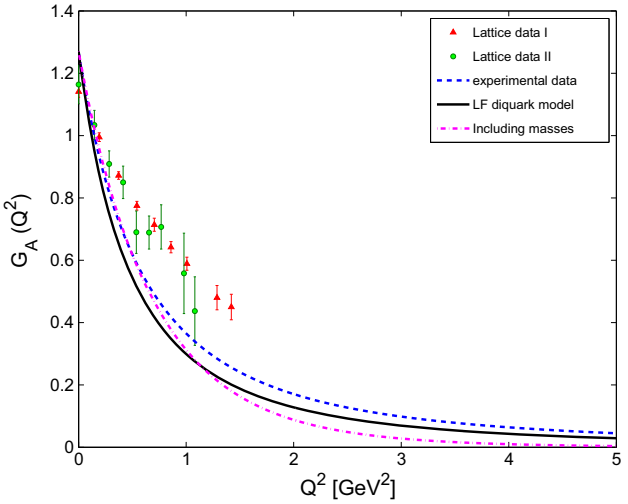

Fig. 4 (Color online) Plot of the axial-vector form factors $G_A(Q^2) = G_A^{u-d}(Q^2)$. The black solid line represents the quark–diquark model in AdS/QCD, the blue dashed line represents dipole fit of experimental data [80] and the data are taken from lattice calculation [82]. The pink dashed-dot line represents the result by including quark and diquark masses in the wave functions (Eq. (23))

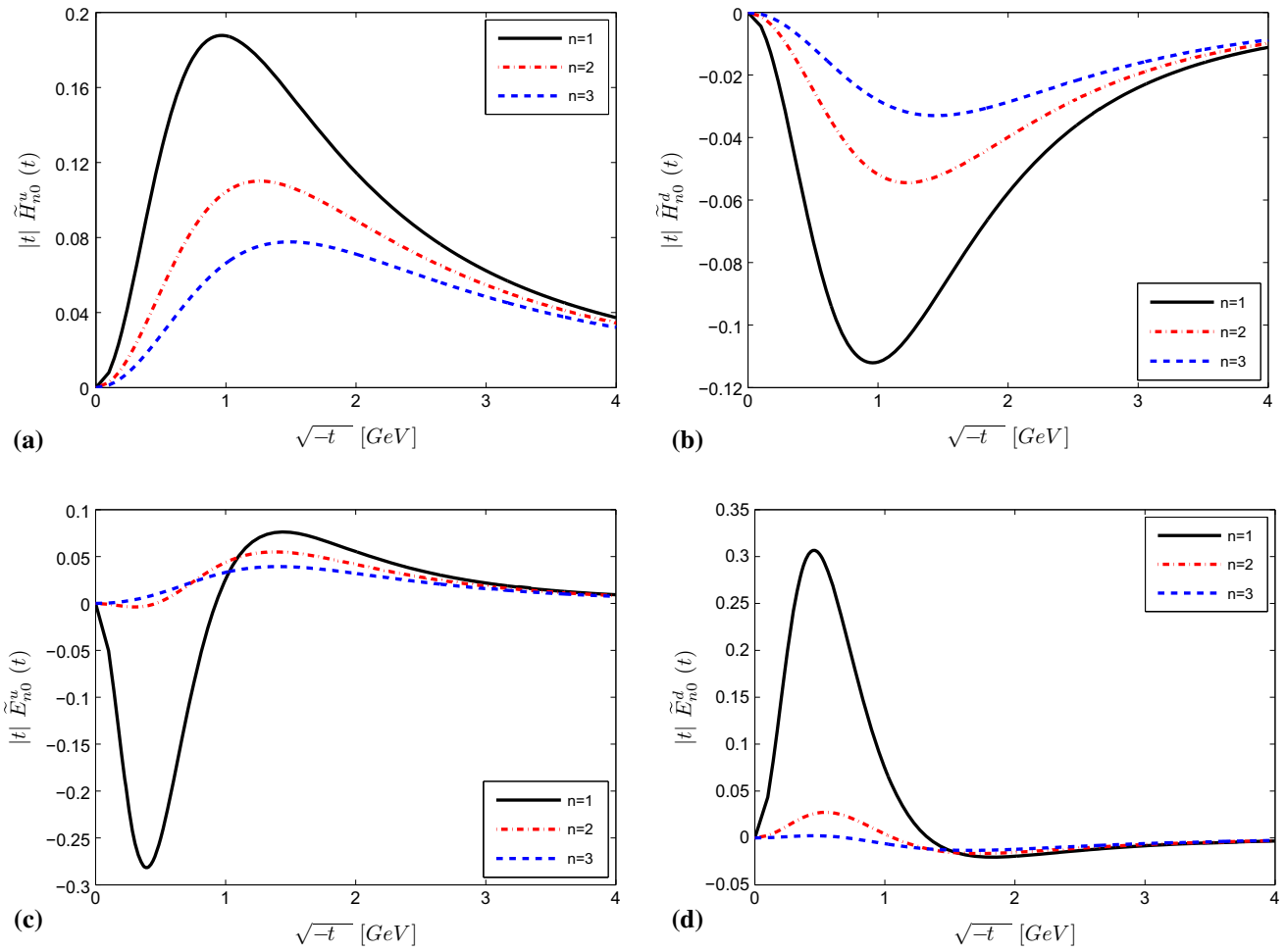

Fig. 5 (Color online) Plots of first three moments of the helicity-dependent GPDs for zero skewness vs. $\sqrt{-t}$ in GeV. The left panel is for the u quark and the right panel is for d quark

The moments of the other GPD, $\widetilde{E}^q_{n0}(t)$, are defined in the same way as (21). The first moments of $\widetilde{H}^q_{n0}(x,0,t)$ and $\widetilde{E}^q_{n0}(x,0,t)$ give the axial-vector form factor, $G^q_A(t)$, and the pseudo-scalar form factor, $G^q_p(t)$, for quark q, respectively. The forward value, $t=0$, of the form factors $g_A = \widetilde{H}_{10}(t=0)$ can be identified as the axial-vector coupling constant (axial charge) [63,80]. Similarly, $g_P = \widetilde{E}_{10}(t=0)$ is known as the pseudo-scalar coupling constant. In Fig. 4, we compare the result for the axial-vector form factors obtained in the quark–diquark model in AdS/QCD with the corresponding results from lattice [82] and the experimental data described by the dipole formula [80]:

$$G_A(Q^2) = \frac{g_A}{(1+Q^2/M_A^2)^2} \tag{22}$$

where the axial-vector coupling constant $g_A = 1.2673$ and the parameter $M_A = 1.069$ GeV, the so-called axial mass [80]. The plot shows that our result is more or less in agreement with the dipole fit of the experimental data. In the same plot, we also compare the result of axial form factor by introducing the mass terms in the wave functions $\varphi^{(i)}_q(x,\mathbf{k}_\perp)$ (Eq. (4)), following Ref. [81]

$$\varphi^{(i)}_q(x,\mathbf{k}_\perp) \sim \exp\left[-\frac{\mathbf{k}^2_\perp}{2\kappa^2}\left\{\frac{\log(1/x)}{(1-x)^2}+\frac{m_q^2}{x}+\frac{m_D^2}{(1-x)}\right\}\right]. \tag{23}$$

Here we use the quark and diquark masses $m_q = 0.35$ GeV and $m_D = 0.65$ GeV, respectively. With the mass terms in the wave functions, the result is in good agreement with the experimental data at low Q^2, however, it deviates at higher Q^2. The second moments of these GPDs correspond to the gravitational form factors of longitudinally polarized quarks in an unpolarized nucleon. The third moments of the GPDs give form factors of a twist-two operator having two covariant derivatives [1,2] and the higher order moments generate the form factors of higher-twist operators. In Fig. 5, the first three moments of the helicity-dependent GPDs $|t|\widetilde{H}^q_{n0}(t)$, $|t|\widetilde{E}^q_{n0}(t)$ as functions of $\sqrt{-t}$ have been shown for the u and d quarks. We observe a strong decrease in the magnitudes of the moments with increasing n. One can understand this

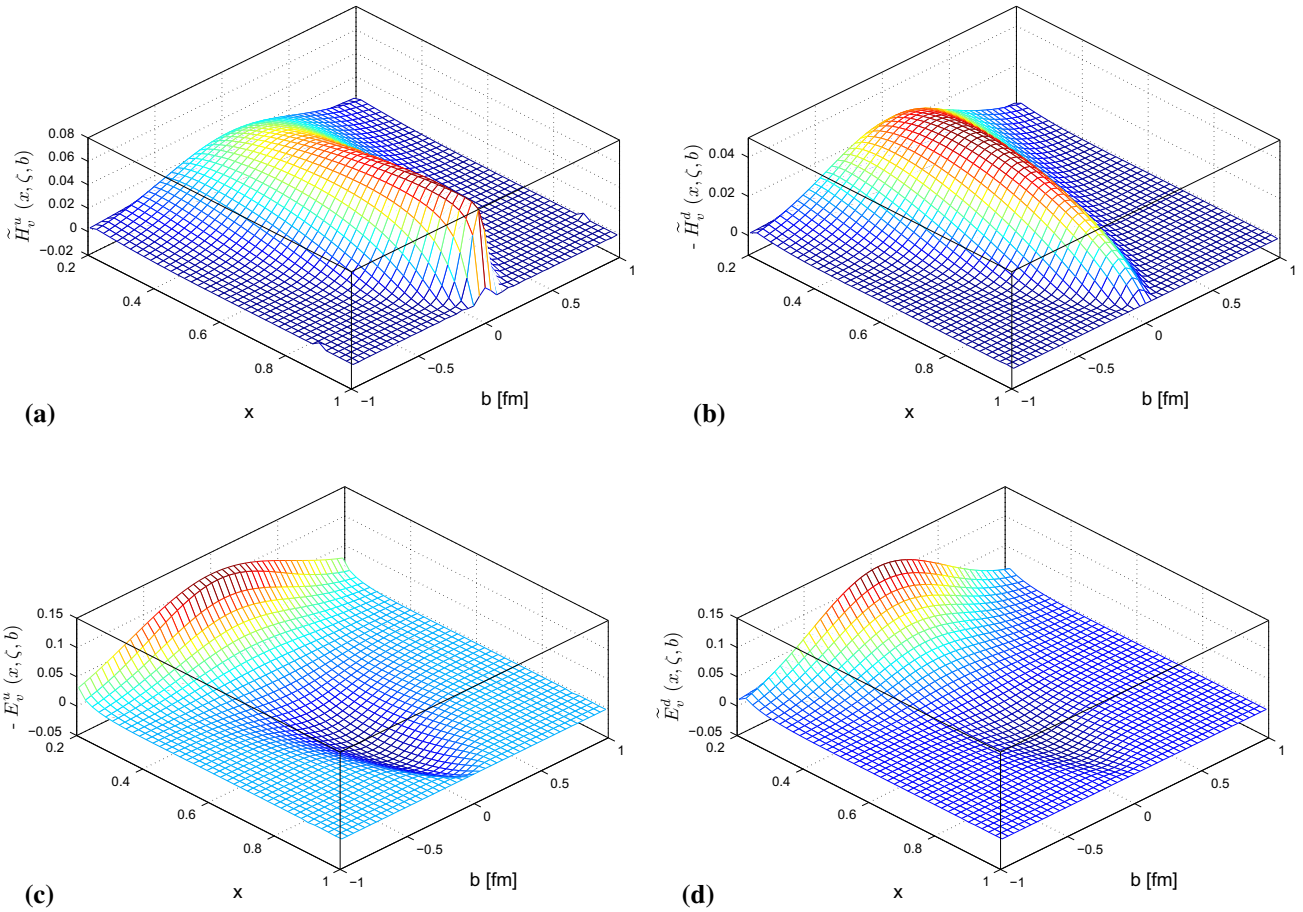

Fig. 6 (Color online) Plots of helicity-dependent GPDs for the nonzero skewness in impact space vs. x and $b = |\mathbf{b}|$ for a fixed value of $\zeta = 0.2$. The left panel is for the u quark and the right panel is for the d quark

aspect from the behavior of the GPDs with x as shown in Fig. 2. Since higher moments involve higher powers of x, the dominant contributions appear from the large x region ($x \to 1$). But the GPDs decrease rapidly as x increases, thus the higher moments become smaller. One can also observe that with increasing index n, the decrease of the moments becomes slower as $-t$ increases. This phenomenon again can be described in terms of the decrease of the GPDs with momentum fraction x, which shows a weaker t slope for the higher moments. A similar behavior of the GPDs has been found in other phenomenological models [19,83,84] and in lattice QCD [61–63,85].

4 Impact parameter representation of helicity-dependent GPDs

4.1 GPDs in transverse impact parameter space

The transverse impact parameter-dependent GPDs are defined by a two-dimensional Fourier transform with respect to the momentum transfer in the transverse direction [5–7,86]:

$$\widetilde{H}^q(x,\zeta,b) = \frac{1}{(2\pi)^2}\int \mathrm{d}^2\boldsymbol{\Delta}_\perp e^{-i\boldsymbol{\Delta}_\perp\cdot\mathbf{b}_\perp}\widetilde{H}^q(x,\zeta,t), \quad (24)$$

$$\widetilde{E}^q(x,\zeta,b) = \frac{1}{(2\pi)^2}\int \mathrm{d}^2\boldsymbol{\Delta}_\perp e^{-i\boldsymbol{\Delta}_\perp\cdot\mathbf{b}_\perp}\widetilde{E}^q(x,\zeta,t), \quad (25)$$

where $\mathbf{b}_\perp$ represents the transverse impact parameter conjugate to the transverse momentum transfer $\boldsymbol{\Delta}_\perp$. For zero skewness, $b = |\mathbf{b}_\perp|$ corresponds a measure of the transverse distance of the struck parton from the center of momentum of the hadron and it follows the condition $\sum_i x_i b_i = 0$, where the sum is over the number of partons. The relative distance between the struck parton and the center of momentum of the spectator system is given by $\frac{|\mathbf{b}_\perp|}{1-x}$, which provides us an estimate of the size of the bound state [87]. For nonzero ζ, the transverse distance of partons from the proton center of momentum differs in the initial and final state, but the relative distance in a hadron stays the same. The transverse positions $\mathbf{b}_\perp$ with the initial and final state proton are shifted relative to each other by an amount of order $\zeta\mathbf{b}_\perp$ [86]. In the DGLAP region $x > \zeta$, the impact parameter $\mathbf{b}_\perp$ describes the location where the quark is pulled out and re-inserted to the proton. In the ERBL domain $x < \zeta$, $\mathbf{b}_\perp$ gives the transverse

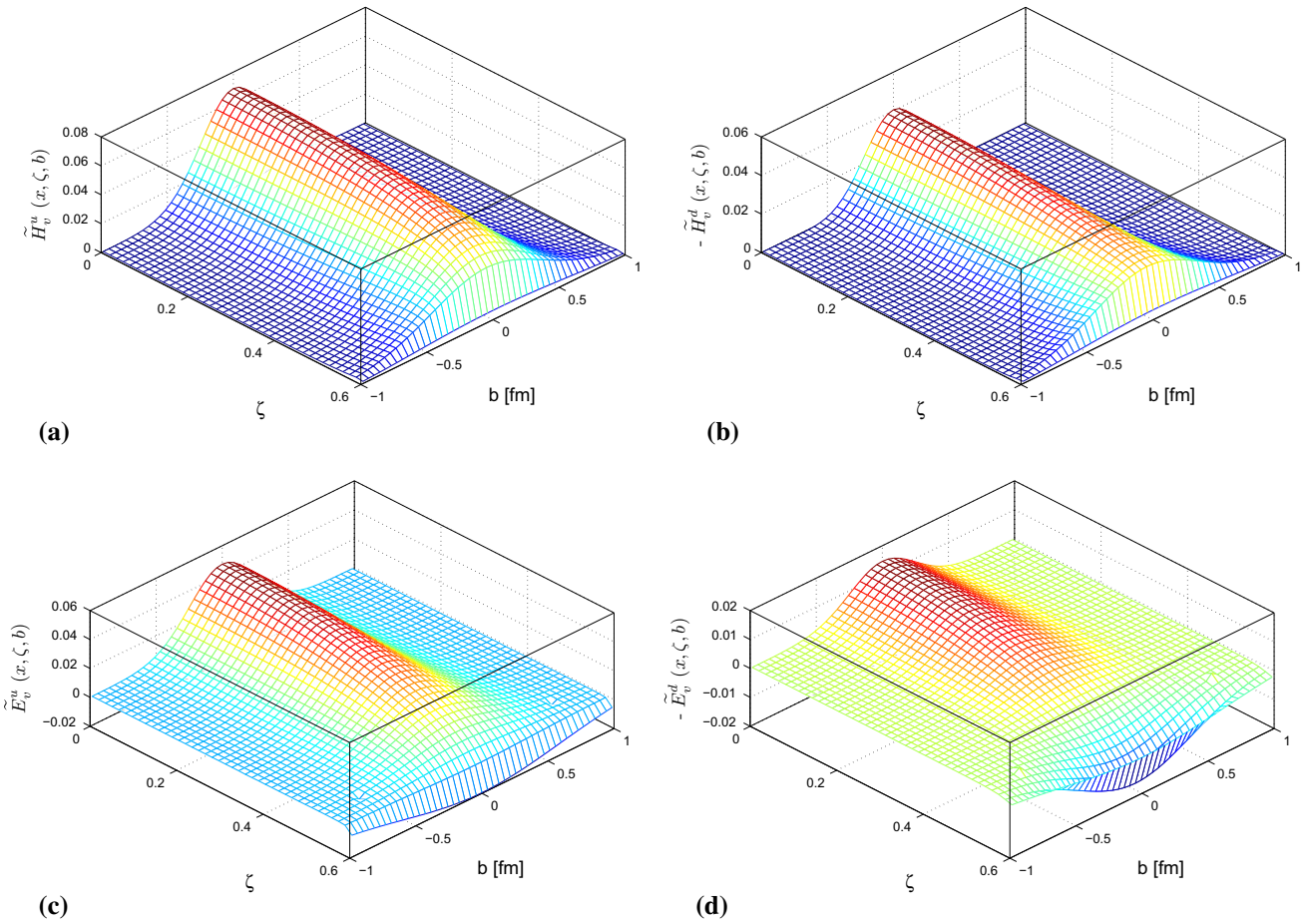

Fig. 7 (Color online) Plots of helicity-dependent GPDs for the nonzero skewness in impact space vs. ζ and $b = |\mathbf{b}|$ for a fixed value of $x = 0.6$. The left panel is for the u quark and the right panel is for the d quark

distance of the quark–antiquark pair inside the proton. For zero skewness, the helicity-dependent GPDs also have a density interpretation in transverse impact parameter space like other GPDs corresponding to the density for longitudinally polarized partons. $\widetilde{H}^q(x, b)$ reflects the density of quarks with helicity equal or opposite to the proton helicity [9–11]. Note that the density interpretation is possible only in the limit $\zeta = 0$, but it is natural to ask what this situation looks like at nonzero ζ, which is applicable for most processes where GPDs can be accessed. Thus, it is interesting to study the helicity-dependent GPDs in the impact parameter space when ζ is nonzero.

In Fig. 6, we show the skewness-dependent GPDs $\widetilde{H}(x, \zeta, b)$ and $\widetilde{E}(x, \zeta, b)$ for u and d quark in transverse impact parameter space for fixed $\zeta = 0.2$ as functions of b and x. Similarly, the GPDs as functions of ζ and b for a fixed value of $x = 0.6$ are shown in Fig. 7. The peak of the distribution $\widetilde{H}(x, \zeta, b)$ for fixed ζ appears at higher x for the u quark whereas it shifts to lower x for the d quark. $\widetilde{E}(x, \zeta, b)$ shows the peaks at lower x for both u and d quarks and one can also observe an oscillatory behavior for the GPDs, $\widetilde{E}(x, \zeta, b)$. This is due to the fact that the GPD in momentum space, $\widetilde{E}(x, \zeta, t)$ has a slight oscillatory behavior as can be seen in Fig. 2b. The width of all the distributions in transverse impact parameter space decreases with increasing x. This implies that the distributions are more localized near the center of momentum for higher values of x. We observe a similar behavior for the u and d quark in $\widetilde{H}(x, \zeta, b)$ and $\widetilde{E}(x, \zeta, b)$ when they are plotted against ζ and b for a fixed values of x in Fig. 7. Another interesting behavior of the GPDs is that, for a fixed value of x, as ζ increases the peaks of all the distributions become broader. This means that as the momentum transfer in the longitudinal direction increases the transverse distance of the longitudinally polarized active quark increases. This is due to the fact that, for nonzero ζ, the relative transverse distance b is shifted by an amount of order ζb [86]. A similar behavior has also been observed in other phenomenological model [16]. We should mention here that the unpolarized, as well as the chiral-odd GPDs also exhibit a similar behavior [18,19]; thus one can conclude that this phenomenon of the GPDs is independent of quark polarization.

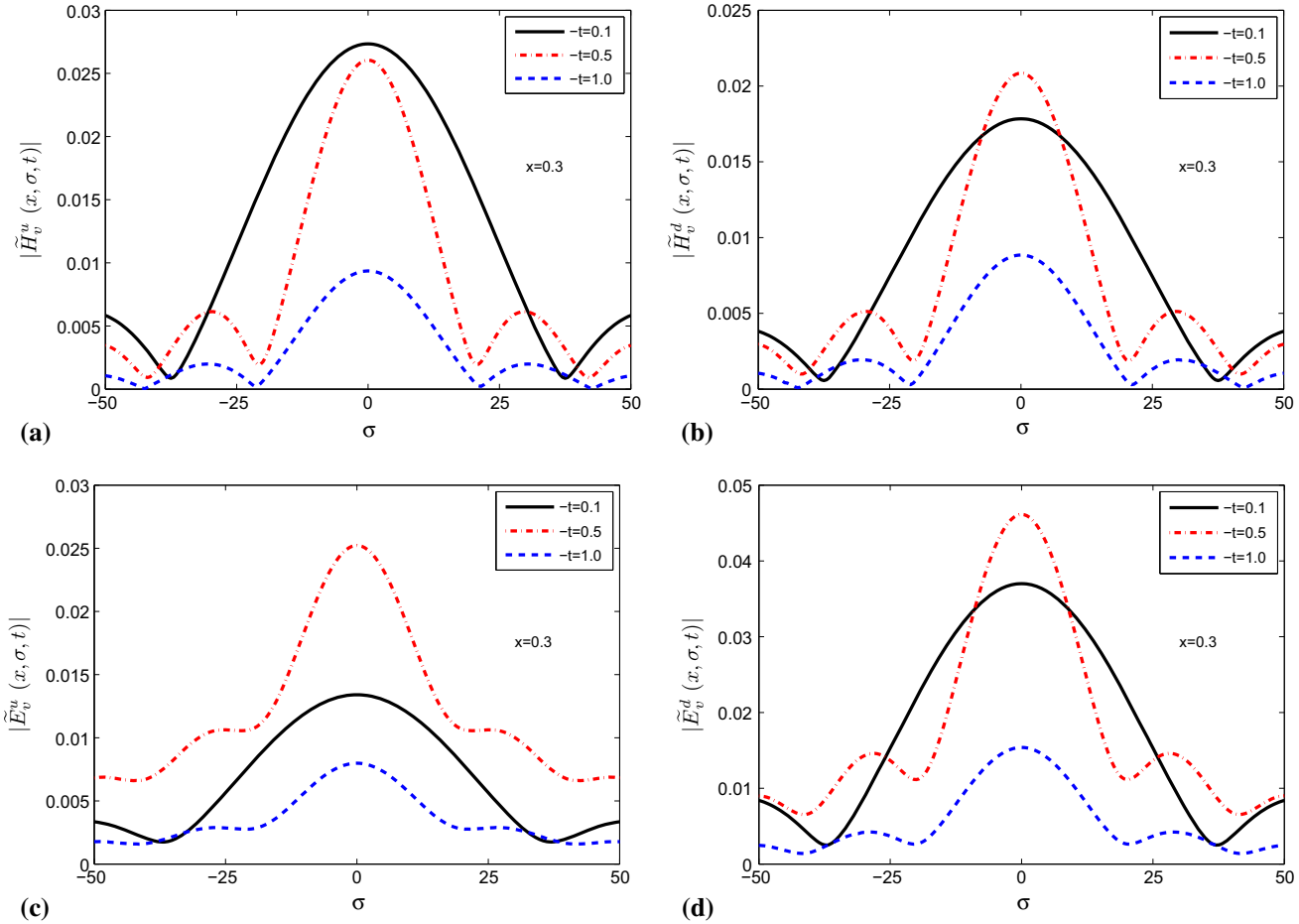

Fig. 8 (Color online) Plots of the helicity-dependent GPDs in longitudinal impact space vs. σ and different values of $-t$ in GeV^2, for a fixed value of $x = 0.3$. The left panel is for u quark and the right panel is for the d quark

4.2 GPDs in longitudinal impact parameter space

The Fourier transform of GPDs with respect to the skewness variable ζ provides a unique way to visualize the structure of the hadron in the boost-invariant longitudinal coordinate space. The boost-invariant longitudinal impact parameter is defined as $\sigma = \frac{1}{2}b^- P^+$, which was first introduced in [14,15]. It has been shown that the DVCS amplitude in a QED model of a dressed electron exhibits an interesting diffraction pattern in the longitudinal impact parameter space in analogous to diffractive scattering of a wave in optics [14,15]. The finite size of the ζ is responsible for producing the diffraction pattern and this can be interpreted as a slit of finite width in equivalent with optics. We should mentioned here that the Fourier transform with a finite range of ζ of any arbitrary function does not provide the diffraction pattern [16]. This pattern depends on the nature of the function. The helicity-dependent GPDs for a photon evaluated in a phenomenological model [60] show similar diffraction patterns in the longitudinal impact parameter space. A certain phenomenological model for proton GPDs exhibits a similar diffraction pattern [16] whereas the GPDs calculated for a simple relativistic spin half system of an electron dressed with a photon display a same pattern in the longitudinal position space [12,17]. A similar phenomenon is also observed for the unpolarized GPDs as well as chiral-odd GPDs in this light-front quark–diquark model [18,19]. In longitudinal position space, the GPDs are defined as

$$\begin{aligned}\widetilde{H}(x,\sigma,t) &= \frac{1}{2\pi}\int_0^{\zeta_f} \mathrm{d}\zeta\, e^{i\zeta P^+ b^-/2}\widetilde{H}(x,\zeta,t),\\ &= \frac{1}{2\pi}\int_0^{\zeta_f} \mathrm{d}\zeta\, e^{i\zeta\sigma}\,\widetilde{H}(x,\zeta,t), \qquad (26)\\ \widetilde{E}(x,\sigma,t) &= \frac{1}{2\pi}\int_0^{\zeta_f} \mathrm{d}\zeta\, e^{i\zeta P^+ b^-/2}\widetilde{E}(x,\zeta,t),\\ &= \frac{1}{2\pi}\int_0^{\zeta_f} \mathrm{d}\zeta\, e^{i\zeta\sigma}\,\widetilde{E}(x,\zeta,t). \qquad (27)\end{aligned}$$

Since the region of our discussion is $\zeta < x < 1$, the upper limit of the ζ integration, ζ_f, is given by $\zeta_{\max}$ if x is larger than $\zeta_{\max}$; otherwise by x if x is smaller than $\zeta_{\max}$ where the maximum value of ζ for a fixed $-t$ is given by

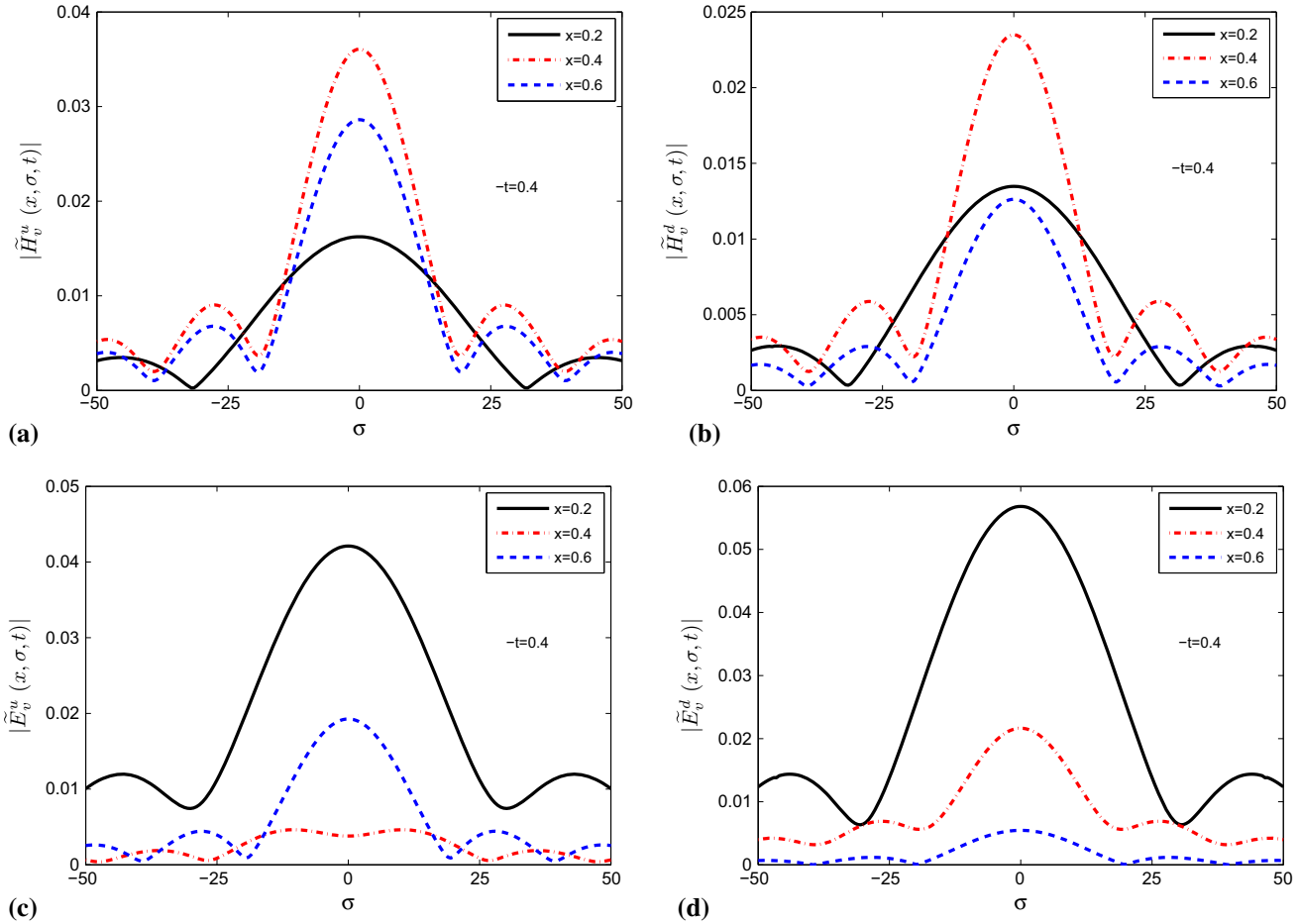

Fig. 9 (Color online) Plots of the chiral-odd GPDs in longitudinal impact space vs. σ and different values of x, for a fixed value of $-t = 0.4$ GeV^2. The left panel is for the u quark and the right panel is for the d quark. For $-t = 0.4$ GeV^2, $\zeta_{\max} \approx 0.307$

$$\zeta_{\max} = \sqrt{\frac{(-t)}{(-t + 4M_n^2)}}. \tag{28}$$

The Fourier spectrum of the helicity-dependent GPDs for u and d quarks in longitudinal position space as a function of σ for different values of $-t$ and fixed $x = 0.3$ are shown in Fig. 8. $\widetilde{H}$ for both u and d quarks displays a diffraction pattern in the σ space as observed for the DVCS amplitude [14,15]. We also observe that $\widetilde{E}(x, \sigma, t)$ for the d quark exhibits the same pattern, but for all values of $-t$, it does not show the prominent pattern for the u quark. This is due to the fact of the distinctly different nature of $\widetilde{E}^u(x, \zeta, t)$ with ζ compared to the other GPDs, which again implies that the diffraction pattern is not solely due to the finite size of the ζ integration, and the functional forms of the GPDs are also important for this phenomenon. The first minima appear at the same values of σ for all the diffraction patterns. In Fig. 9, we also show the GPDs in σ space for different values of x and fixed $-t = 0.4$ GeV^2. Here ζ_f plays the role of the slit width, equivalent to the single slit optical diffraction pattern. Since the positions of the minima are inversely proportional to the slit width, as the slit width ζ_f increases, the minima shift towards the center of the diffraction pattern.

4.3 Quark transverse distributions

One can access the probability $\rho^q(b, \lambda, \Lambda)$ to find a quark with transverse position b and light-cone helicity λ $(= \pm 1)$ in the nucleon with longitudinal polarization Λ $(= \pm 1)$ via the Fourier transform of the combination of the Dirac and axial form factors of the quark as [11,52,88]

$$\begin{aligned}\rho^q(b, \lambda, \Lambda) &= \frac{1}{2}\int \mathrm{d}^2\mathbf{\Delta}_\perp \left[F_1^q(Q^2) + \lambda\Lambda G_A^q(Q^2)\right] e^{i\mathbf{\Delta}_\perp\cdot\mathbf{b}_\perp} \\ &= \frac{1}{4\pi}\int \mathrm{d}Q\, Q J_0(Qb)\left[F_1^q(Q^2) + \lambda\Lambda G_A^q(Q^2)\right] \\ &\equiv \frac{1}{2}\left[\rho^q(b) + \lambda\Lambda\Delta q(b)\right],\end{aligned} \tag{29}$$

where $\rho^q(b)$ and $\Delta q(b)$ are the Fourier transforms of $F_1^q(Q^2)$ and $G_A^q(Q^2)$, respectively, and J_0 is a cylindrical Bessel function. $\rho^q(b)$ corresponds to $d(b)$, the charge density for the d quark and $2u(b)$, twice charge density for u

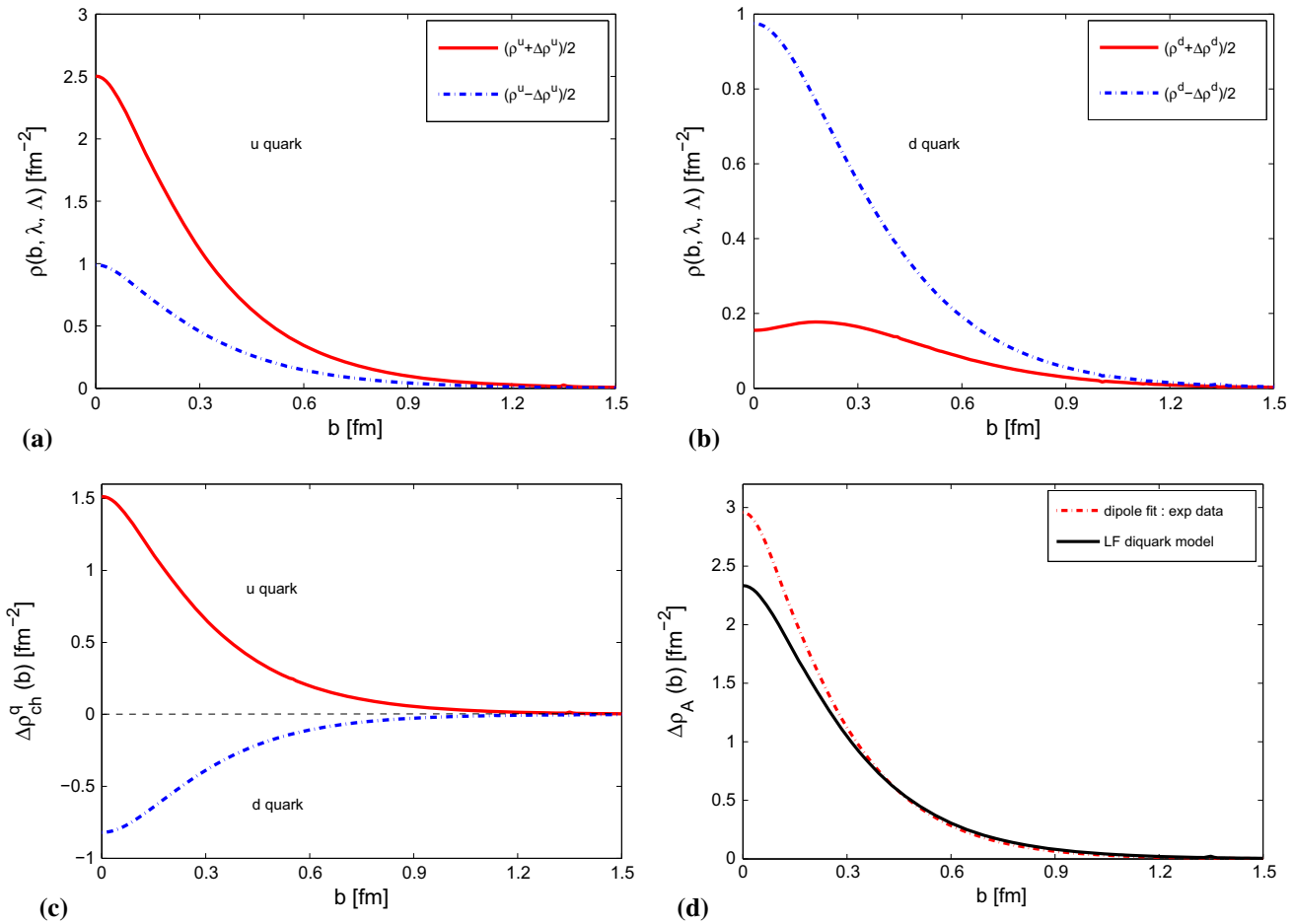

Fig. 10 (Color online) Plots of the transverse distribution of u and d quarks in a longitudinally polarized proton as a function of the impact parameter b. The total contribution for **a** the u quark, and **b** the d quark when quarks are polarized in the longitudinal direction, either parallel (solid red lines) or anti-parallel (dashed blue lines) with respect to the proton helicity. **c** The axial contributions Δu and Δd for the u and d quarks. **d** The axial distribution $\rho_A(b) = \Delta u(b) - \Delta d(b)$ (solid black line) in comparison with the distribution from the dipole fit of experimental data for axial form factor (red dashed dot)

quark [18,88]. The normalizations of $\rho^q(b)$ and $\Delta q(b)$ are $\int \mathrm{d}^2b\ \rho^q(b) = n_q$, where $n_u = 2$, $n_d = 1$ in a proton and $\int \mathrm{d}^2b\ \Delta q(b) = \Delta q$, where Δq is the axial charge of quark q. We show the resulting probability for the u and d quarks considering a positive proton helicity ($\Lambda = 1$) in Fig. 10a, b, respectively. The axial contributions $\Delta u(b)$ and $\Delta d(b)$ for the u and d quarks having opposite signs are shown in Fig. 10c, whereas the transverse distribution $\rho^q(b)$, which is positive for both u and d, in this light-front quark–diquark model can be found in [18]. The difference between $\Delta u(b)$ and $\Delta d(b)$ is compared with the distribution obtained from the dipole fit of axial form factor in Fig. 10d. One can notice that though there is a mismatch at $b = 0$, at larger b, the light-front quark–diquark model agrees well the result obtained from the dipole fit. Since $\Delta u(b)$ is positive but $\Delta d(b)$ is negative, the probability to find a u quark with positive helicity is maximal when it is aligned with the proton helicity, while the opposite occurs for the d quarks.

5 Summary

In the present work, we have studied the helicity-dependent GPDs for u and d quark in proton for nonzero skewness in the light-front quark–diquark model predicted by the soft-wall AdS/QCD. We have obtained the GPDs in terms of the overlaps of the light-front wave functions considering the DGLAP region i.e., for ($x > \zeta$). We have observed that for fixed ζ. The peaks of the distributions move to higher values of x with increasing of $-t$; again the heights of the peaks increase and also shift to higher values of x as ζ increases for fixed $-t$. We also observed markedly different behavior for $\widetilde{E}$ for the u quark from the other GPDs in this model when we plot the GPDs against ζ for different $-t$ and fixed x. It shows that with increasing ζ, $\widetilde{E}^u$ started to increase smoothly from different values at $\zeta = 0$ for different values of $-t$ but the magnitude at $\zeta_{\max}$ decreases with increasing $-t$ whereas for the other GPDs, the magni-

tude at $\zeta_{\max}$ increases with increasing $-t$. The axial form factor has been evaluated in this quark–diquark model and compared with the dipole fit of experimental data as well as lattice data. It shows that our result is more or less in agreement with the experimental data and better compared to lattice.

We have also presented all the helicity-dependent GPDs in the transverse impact parameter (b) as well as longitudinal position(σ) spaces by taking the Fourier transform of the GPDs with respect to momentum transfer in the transverse direction ($\mathbf{\Delta}_\perp$), and skewness (ζ), respectively. For zero skewness, the impact parameter b gives a measure of the transverse distance between the struck parton and the center of momentum of the hadron. In this model, the GPD $\widetilde{H}$ shows a quite different behavior in the transverse impact parameter space for the u and d quarks when plotted in x and b but for $\widetilde{E}$, the behaviors for both u and d quark are almost same. Again, the nature of $\widetilde{H}$ is more or less the same when plotted against ζ and b, but $\widetilde{E}$ shows a different behavior for the u and d quark. With increasing ζ or decreasing x, the widths of all distributions increase. It has been found that the GPDs in σ space show diffraction patterns analogous to diffractive scattering of a wave in optics. A similar diffraction pattern also has been observed in several other models. The diffraction patterns for both u and d quarks are of the same qualitative nature. The general features of this phenomenon are mainly depending on the finiteness of the ζ integration but the dependence of GPDs on x, ζ and t is also crucial. Like other GPDs, $\widetilde{E}$ for the u quark does not show the diffraction pattern for all values of $-t$. This is due to a different behavior of $\widetilde{E}^u$ with ζ from the other GPDs which also indicates that the diffraction pattern is not solely due to finiteness of ζ integration and the functional behaviors of the GPDs are important to have the phenomenon. In this model, we have also studied the transverse distributions of quark with light-cone helicities $\lambda(=\pm 1)$ in the nucleon with longitudinal polarization $\Lambda(=+1)$. We observed that when the helicity of the u quark is aligned with the proton helicity, the probability to find it is maximal but the situation is opposite for the d quark.

Funded by SCOAP[3].

References

1. For reviews on generalized parton distributions, and DVCS, see M. Diehl, Phys. Rep. **388**, 41 (2003)
2. A.V. Belitsky, A.V. Radyushkin, Phys. Rep. **418**, 1 (2005)
3. K. Goeke, M.V. Polyakov, M. Vanderhaeghen, Prog. Part. Nucl. Phys. **47**, 401 (2001)
4. M. Burkardt, Phys. Rev. D **72**, 094020 (2005)
5. M. Burkardt, Int. J. Mod. Phys. A **18**, 173 (2003)
6. M. Burkardt, Phys. Rev. D **62**, 071503 (2000). Erratum-ibid. Phys. Rev. D **66**, 119903 (2002)
7. J.P. Ralston, B. Pire, Phys. Rev. D **66**, 111501 (2002)
8. X. Ji, Phys. Rev. Lett. **78**, 610 (1997)
9. S. Boffi, B. Pasquini, Riv. Nuovo Cim. **30**, 387 (2007)
10. M. Diehl, P. Hagler, Eur. Phys. J. C **44**, 87 (2005)
11. B. Pasquini, S. Boffi, Phys. Lett. B **653**, 23 (2007)
12. D. Chakrabarti, R. Manohar, A. Mukherjee, Phys. Rev. D **79**, 034006 (2009)
13. H. Dahiya, A. Mukherjee, Phys. Rev. D **77**, 045032 (2008)
14. S.J. Brodsky, D. Chakrabarti, A. Harindranath, A. Mukherjee, J.P. Vary, Phys. Lett. B **641**, 440 (2006)
15. S.J. Brodsky, D. Chakrabarti, A. Harindranath, A. Mukherjee, J.P. Vary, Phys. Rev. D **75**, 014002 (2007)
16. R. Manohar, A. Mukherjee, D. Chakrabarti, Phys. Rev. D **83**, 014004 (2011)
17. N. Kumar, H. Dahiya, Int. J. Mod. Phys. A **30**(02), 1550010 (2015)
18. C. Mondal, D. Chakrabarti, Eur. Phys. J. C **75**(6), 261 (2015)
19. D. Chakrabarti, C. Mondal, Phys. Rev. D **92**(7), 074012 (2015)
20. X.D. Ji, Phys. Rev. D **55**, 7114 (1997)
21. A.V. Radyushkin, Phys. Rev. D **56**, 5524 (1997)
22. A. Airapetian et al. [HERMES Collaboration], Phys. Rev. Lett. **87**, 182001 (2001)
23. S. Stepanyan et al. [CLAS Collaboration], Phys. Rev. Lett. **87**, 182002 (2001)
24. C.M. Camacho et al. [Jefferson Lab Hall A and Hall A DVCS Collaborations], Phys. Rev. Lett. **97**, 262002 (2006)
25. S. Chen et al. [CLAS Collaboration], Phys. Rev. Lett. **97**, 072002 (2006)
26. F.X. Girod et al. [CLAS Collaboration], Phys. Rev. Lett. **100**, 162002 (2008)
27. M. Mazouz et al. [Jefferson Lab Hall A Collaboration], Phys. Rev. Lett. **99**, 242501 (2007)
28. S. Chekanov et al. [ZEUS Collaboration], Phys. Lett. B **573**, 46 (2003)
29. A. Aktas et al. [H1 Collaboration], Eur. Phys. J. C **44**, 1 (2005)
30. A. Airapetian et al. [HERMES Collaboration], Phys. Rev. D **75**, 011103 (2007)
31. F.D. Aaron et al. [H1 Collaboration], Phys. Lett. B **659**, 796 (2008)
32. A. Airapetian et al. [HERMES Collaboration], Phys. Lett. B **704**, 15 (2011)
33. A. Airapetian et al. [HERMES Collaboration], JHEP **0806**, 066 (2008)
34. A. Airapetian et al. [HERMES Collaboration], Nucl. Phys. B **842**, 265 (2011)
35. C. Adolph et al. [COMPASS Collaboration], Nucl. Phys. B **915**, 454 (2017)
36. C. Adolph et al. [COMPASS Collaboration], Phys. Lett. B **731**, 19 (2014)
37. R. Enberg, B. Pire, L. Szymanowski, Eur. Phys. J. C **47**, 87 (2006)
38. DYu. Ivanov, B. Pire, L. Szymanowski, O.V. Teryaev, Phys. Lett. B **550**, 65 (2002)
39. DYu. Ivanov, B. Pire, L. Szymanowski, O.V. Teryaev, Phys. Part. Nucl. **35**, 67 (2004)
40. S.V. Goloskokov, P. Kroll, Eur. Phys. J. A **47**, 112 (2011)
41. S.V. Goloskokov, P. Kroll, Eur. Phys. J. C **74**, 2725 (2014)
42. X.D. Ji, W. Melnitchouk, X. Song, Phys. Rev. D **56**, 5511 (1997)
43. I.V. Anikin, D. Binosi, R. Medrano, S. Noguera, V. Vento, Eur. Phys. J. A **14**, 95 (2002)
44. V.Y. Petrov, P.V. Pobylitsa, M.V. Polyakov, I. Bornig, K. Goeke, C. Weiss, Phys. Rev. D **57**, 4325 (1998)

45. M. Penttinen, M.V. Polyakov, K. Goeke, Phys. Rev. D **62**, 014024 (2000)
46. B.C. Tiburzi, G.A. Miller, Phys. Rev. C **64**, 065204 (2001)
47. B.C. Tiburzi, G.A. Miller, Phys. Rev. D **65**, 074009 (2002)
48. A. Mukherjee, M. Vanderhaeghen, Phys. Rev. D **67**, 085020 (2003)
49. S. Scopetta, V. Vento, Phys. Rev. D **69**, 094004 (2004)
50. S. Scopetta, V. Vento, Eur. Phys. J. A **16**, 527 (2003)
51. S. Boffi, B. Pasquini, M. Traini, Nucl. Phys. B **649**, 243 (2003)
52. B. Pasquini, M. Pincetti, S. Boffi, Phys. Rev. D **72**, 094029 (2005)
53. A. Vega, I. Schmidt, T. Gutsche, V.E. Lyubovitskij, Phys. Rev. D **83**, 036001 (2011)
54. A. Vega, I. Schmidt, T. Gutsche, V.E. Lyubovitskij, Phys. Rev. D **85**, 096004 (2012)
55. D. Chakrabarti, C. Mondal, Phys. Rev. D **88**, 073006 (2013)
56. M. Rinaldi, Phys. Lett. B **771**, 563 (2017)
57. M.C. Traini, Eur. Phys. J. C **77**(4), 246 (2017)
58. S. Boffi, B. Pasquini, M. Traini, Nucl. Phys. B **680**, 147 (2004)
59. S. Scopetta, V. Vento, Phys. Rev. D **71**, 014014 (2005)
60. A. Mukherjee, S. Nair, Phys. Lett. B **707**, 99 (2012)
61. M. Gockeler et al. [QCDSF Collaboration and UKQCD Collaboration], Phys. Rev. Lett. **98**, 222001 (2007)
62. M. Gockeler et al., Phys. Lett. B **627**, 113 (2005)
63. P. Hagler, Phys. Rep. **490**, 49 (2010)
64. P. Hagler, Phys. Lett. B **594**, 164 (2004)
65. J.D. Bratt et al. [LHPC Collaboration], Phys. Rev. D **82**, 094502 (2010)
66. T. Gutsche, E.L. Valery, I. Schmidt, A. Vega, Phy. Rev. D **89**, 054033 (2014)
67. S.J. Brodsky, G.F. de Teramond, Phys. Rev. D. **77**, 056007 (2008)
68. S.J. Brodsky, G.F. de Téramond, arXiv:1203.4025 [hep-ph]
69. D. Chakrabarti, C. Mondal, A. Mukherjee, Phys. Rev. D **91**(11), 114026 (2015)
70. C. Mondal, N. Kumar, H. Dahiya, D. Chakrabarti, Phys. Rev. D **94**(7), 074028 (2016)
71. D. Chakrabarti, C. Mondal, Eur. Phys. J. A **52**(9), 285 (2016)
72. C. Mondal, D. Chakrabarti, Few Body Syst. **57**(8), 723 (2016)
73. D. Chakrabarti, T. Maji, C. Mondal, A. Mukherjee, Eur. Phys. J. C **76**(7), 409 (2016)
74. T. Maji, C. Mondal, D. Chakrabarti, O.V. Teryaev, JHEP **1601**, 165 (2016)
75. A. Bacchetta, S. Cotogno, B. Pasquini, Phys. Lett. B **771**, 546 (2017)
76. D. Chakrabarti, C. Mondal, Eur. Phys. J. C **73**, 2671 (2013)
77. M. Diehl, Eur. Phys. J. C **19**, 485 (2001)
78. C. Lorc, Phys. Lett. B **735**, 344 (2014)
79. E. Leader, A.V. Sidorov, D.B. Stamenov, Phys. Rev. D **82**, 114018 (2010)
80. V. Bernard, L. Elouadrhiri, U.G. Meissner, J. Phys. G **28**, R1 (2002)
81. S.J. Brodsky, G.F. de Teramond, Subnucl. Ser. **45**, 139 (2009)
82. C. Alexandrou, M. Constantinou, S. Dinter, V. Drach, K. Jansen, C. Kallidonis, G. Koutsou, Phys. Rev. D **88**(1), 014509 (2013)
83. N. Sharma, Phys. Rev. D **90**, 095024 (2014)
84. M. Diehl, T. Feldmann, R. Jakob, P. Kroll, Eur. Phys. J. C **39**, 1 (2005)
85. P. Hagler et al. [LHPC Collaboration], Phys. Rev. D **77**, 094502 (2008)
86. M. Diehl, Eur. Phys. J. C **25**, 223 (2002). Erratum: [Eur. Phys. J. C **31**, 277 (2003)]
87. M. Diehl, T. Feldman, R. Jacob, P. Kroll, Eur. Phys. J. C **39**, 1 (2005)
88. B. Pasquini, S. Boffi, Phys. Rev. D **76**, 074011 (2007)